2005 American Control Conference
June 8-10, 2005. Portland, OR, USA

Validation of Simplified Formation Models at L2

Isaac Miller and Mark Campbell
Sibley School of Mechanical and Aerospace Engineering
Cornell University, Ithaca NY, 14853
{itm2, mc288}@cornell.edu

Abstract— **This paper introduces a new method to probabilistically evaluate the validity of dynamics model approximations, and applies the method to simplified models of satellite formation dynamics near the Sun - Earth / Moon L2 libration point. The new method uses a Monte Carlo scheme similar to a *Sampling Importance Resampling* filter to evolve state probability densities through satellite dynamics models of varying complexity. The evolved densities are fit with a Gaussian mixture model and compared probabilistically to evaluate the validity of the dynamics models over time.**

I. Introduction

The gravitational field created by two large bodies acting on a small satellite is known to have five equilibrium or *libration* points [1]. The environment at these libration points is favorable for long duration missions, and in particular the L2 point is well-suited for future space telescopes [2]. Many of these telescopes consist of several free flying components and require varying degrees of precision formation flying. These missions can typically be decomposed into two formation control topologies: formation maneuvering, where a new science focus is selected and the formation must change its motion or shape, and formation keeping, where the formation maintains its shape for scientific data collection. Unfortunately, the satellite dynamics near the L2 point are nonlinear, making it difficult to design controllers to maintain individual satellites within these formation control topologies. In order to regain use of the most successful tools for controller design, a simplified linear model of satellite dynamics is sometimes assumed for short periods of time, i.e. during formation keeping [3].

One common model of relative dynamics between two satellites is the double integrator, in which all external forces are assumed to have the same influence on both satellites [3]. Under this model, the satellites' thrusters are the only forces that cause relative motion between members of the formation, and it is easy to design fuel-optimal controllers [4]. In Ref. [3], the validity of this model has been explored using a bounding technique for orbits under the primary influence of the Sun. The goals in this study are to:

1) Explore the validity of simplified models in the L2 environment to aid the increasing number of potential missions at the L2 point.
2) Characterize the accuracy of the double integrator approximation in terms of error probabilities.
3) Develop insight into how the nonlinearities of the L2 point influence uncertainty propagation between the true and approximate models.

The approach of this work is as follows. Several dynamics models of varying complexity are developed to approximate satellite dynamics at the L2 point. These models are tested by comparing the uncertainty of a satellite driven by both disturbance forces and initial measurement uncertainty. In order to characterize the uncertainty environment for each of these models, a Monte Carlo method similar to the SIR or *Sampling Importance Resampling* filter is used to evolve satellite state probability distributions in each model. These distributions are used to characterize the probabilistic evolution of model errors over time.

This paper is outlined as follows. In sections II-A through II-C particle filters are reviewed, including how they may be used to evolve probability distributions through complex dynamics models. In section II-D, evolved probability probability distributions are shown to be able to characterize the accuracy of approximations to those dynamics models. In section III, the method is used to characterize the accuracy of the double integrator approximation to relative dynamics of satellites near the L2 point.

II. Particle Filters as a Method for Propagating State Probability Distributions

A. Model Assumptions

It is first necessary to state all assumptions made in creating the dynamics models to be compared in this work. First, it is assumed that the dynamics of all systems are written in a possibly nonlinear continuous time equation of the form:

$$\dot{\vec{x}}(t) = f(\vec{x}(t)) + B_{cts}(t)\vec{w}_{cts}(t) \qquad (1)$$

where $\vec{x}(t) \in \Re^N$ is the system consisting of positions and velocities along each coordinate axis, the column vector $\vec{w}_{cts}(t)$ is an exogenous disturbance to the system, and the function f is the dynamics function and may be nonlinear. The subscript cts is used to denote the continuous time representations of the noise input matrix. It is also assumed that the noise $\vec{w}_{cts}(t)$ enters linearly into the right hand side of equation (1) through the matrix $B_{cts}(t)$. When necessary, the continuous time dynamics can be approximated as a discrete time difference equation of the form:

$$\vec{x}(t_{k+1}) = \int_{t_k}^{t_{k+1}} f\big(\vec{x}(t_k)\big)dt + B(t_k)\vec{w}(t_k) \qquad (2)$$

I. Miller: Graduate Research Fellow
M. Campbell: Associate Professor, Senior Member of AIAA

0-7803-9098-9/05/$25.00 ©2005 AACC

where k is an integer time index, dt the sampling period, and $B(t_k)$, $\vec{w}(t_k)$ are equivalent discrete time representations of the input matrix $B_{cts}(t)$ and process noise $\vec{w}_{cts}(t)$.

In this paper, all dynamics models are given in continuous form as in equation (1). Noise is simulated either as the continuous form of the dynamics given in equation (1) or as the discrete form given in equation (2). It will be made clear which model is used in each simulation by representing the time dependency t_k in discrete time systems by its index k alone; for example. It is also assumed that the input matrix B is constant. For satellite simulations, it is assumed that the initial state error covariance matrix $P(0) = E\big[\big(\vec{x}(0) - \bar{x}(0)\big)\big(\vec{x}(0) - \bar{x}(0)\big)^T\big]$ is known as a property of the satellite's sensors. Furthermore, the satellite's initial distribution is assumed to be Gaussian.

B. Evolution of Probability Distributions

In order to characterize the uncertainty near the L2 libration point for different model types, it is necessary to evolve satellite uncertainty under the possibly nonlinear dynamics function f. Although there is no exact method for evolving a probability distribution through a nonlinear transformation, particle filters have been demonstrated successfully as an approximate method on a wide variety of nonlinear systems and non-Gaussian distributions [5]. Particle filters approximate a true probability distribution with a finite set of weighted particles, often chosen according to a Monte Carlo scheme [6]. By evolving particles through a dynamics function with simulated process noise, particle filters are able to construct an approximation to the state probability distribution $p(\vec{x})$ at any time k of interest:

$$p(\vec{x}(k)) \approx \sum_{i=1}^{N} W_i(k)\delta\Big(\vec{x}(k) - \vec{x}_i(k)\Big) \tag{3}$$

where $W_i(k)$ are the weights of each of the particles $\vec{x}_i(k)$, and $\delta(\cdot)$ is the Dirac delta function. The weights are always normalized so the set of particles and weights constitutes a discrete probability distribution. The important result in particle filter literature is that as $N \to \infty$, the probability distribution approaches the true distribution [6]. The motivation for using a particle filter in this context lies in the fact that it gives significant information on the shape of the true distribution, allowing better evolution and interpretation of model error dynamics at the L2 point.

C. The SIR Filter

Most particle filters share the following set of common steps [5]. First, a set of N particles $\vec{x}_i(k)$ is selected at random according to a known initial probability distribution of the system state. Next, each particle is given a weight $W_i(k)$. The particles are then evolved according to the dynamics of equation (2) to some arbitrary time. When a new measurement is available, the particle filter adjusts the weights to emphasize those that are more likely to represent the true state. For this study, however, the focus is on the evolution of the distribution, so there are no measurements. As a result, weights on all particles remain constant, as any resampling or reweighting would degrade the model's performance. This matches the first few steps of the SIR or *Sampling Importance Resampling* filter, without the reweighting and resampling steps [6]. A list of steps is given in Table I.

TABLE I

STEPS TO ESTIMATE THE EVOLUTION OF THE STATE DISTRIBUTION

1) Pick a set of N particles $\vec{x}_i(0)$ according to the known initial Gaussian distribution with error covariance $P(0)$.
2) Numerically integrate each particle according to f for the sample period dt. If the process noise $\vec{w}_i$ is modeled with continuous dynamics, include $\vec{w}_i$ in the integration and skip step 3.
3) Pick a set of N process noise vectors $\vec{w}_i$ according to the noise distribution. Perturb each particle $\vec{x}_i(k)$ by adding one noise vector to it. The new set of perturbed particles represent $\vec{x}_i(k+1)$, a single evolution of the old particles according to the discrete time dynamics of equation (2).
4) Repeat from step 2 for the desired simulation time. When finished, the set of particles are a discrete approximation of the true state probability matrix [6].

D. Error and Probability Calculations

The algorithm of Table I is a method to propagate an initial uncertainty distribution through a dynamics model of the form given by equation (2). If more than one dynamics model exists for a system, the evolution method of the previous section can be used to compare the two models probabilistically. Consider two models attempting to represent a particular system:

$$\begin{aligned} \vec{x}_1(k+1) &= f_1\big(\vec{x}_1(k)\big) + B\vec{w}(k) \\ \vec{x}_2(k+1) &= f_2\big(\vec{x}_2(k)\big) + B\vec{w}(k) \end{aligned} \tag{4}$$

These models have identical input matrices and noise models but different dynamics functions. The two models may represent a highly complex nonlinear model for evaluation and a simplified model for design. If these systems begin with the same particles and are driven by the same process noise, then any differences in the evolution of the particles can only be caused by differences in the underlying dynamics functions. The i^{th} evolved particle $\vec{x}_{i,1}(k)$ from system 1 can be subtracted from the evolved particles $\vec{x}_{i,2}(k)$ from system 2 particle by particle to give the i^{th} error vector:

$$\vec{e}_i(k) = \vec{x}_{i,1}(k) - \vec{x}_{i,2}(k) = \begin{pmatrix} \vec{e}_i^{\,p} \\ \vec{e}_i^{\,v} \end{pmatrix} \tag{5}$$

where $\vec{e}_i^{\,p}$ is the error vector of just the position states of the i^{th} particle, and $\vec{e}_i^{\,v}$ is the error vector of just the velocity states of the i^{th} particle. The evolution of the distribution of these error vectors gives valuable insight into the differences between the two system models.

Apart from the error vectors' discrete distribution, additional analysis and insight can be found by considering the distributions of the scalar magnitudes of position errors and velocity errors separately. In particular, the position and

velocity error magnitudes of the particles, e_i^p and e_i^v, may be used to create two Gaussian mixture models that represent the position and velocity error distributions with sums of M Gaussians [7]. The two Gaussian mixture model probability densities are continuous densities in the magnitudes of position and velocity error, e^p and e^v, respectively. For the position error, the density is written:

$$P_p(e^p) = \sum_{j=1}^{M} \alpha_j N_j(e^p) \tag{6}$$

where α_j is a weighting coefficient and $N_j(e^p) \sim N(\mu_j, \sigma_j)$ is the j^{th} Gaussian distribution of mean μ_i and standard deviation σ_i evaluated at the point e^p. The probability density function for velocity error magnitude e^v is defined in an analogous manner. A typical expectation maximization algorithm as described in [7] can be used to set the weighting coefficients and the mean and standard deviation of the component Gaussians. First the likelihood of each initial component given each particle's error e_i^p is determined using Bayes' theorem:

$$P(j|e_i^p) = \frac{\alpha_j N_j(e_i^p)}{\sum_{L=1}^{M} \alpha_L N_L(e_i^p)}$$

Next, the component Gaussians and weights are updated:

$$\hat{\alpha}_j = \sum_{i=1}^{N} P(j|e_i^p) \tag{7}$$

$$\hat{\mu}_j = \frac{\sum_{i=1}^{N} x_i P(j|e_i^p)}{\sum_{i=1}^{N} P(j|e_i^p)} \tag{8}$$

$$\hat{\sigma}_j^2 = \frac{\sum_{i=1}^{N} (e_i^p - \hat{\mu}_j)^2 P(j|e_i^p)}{\sum_{i=1}^{N} P(j|e_i^p)} \tag{9}$$

These steps are then iterated until convergence. A typical metric used to measure convergence of the Gaussian mixture model is the log likelihood function [7]. The log likelihood function at the k^{th} iteration is:

$$LL_k = \sum_{i=1}^{N} \log\left(\sum_{j=1}^{M} \alpha_j N_j(e_i^p)\right) \tag{10}$$

where the values of α_j and $N_j(\cdot)$ are taken from the mixture model at the k^{th} iteration. The mixture model is then iterated using equations (7) - (9) until the log likelihood changes by less than 1% between successive iterations, or until a max number of iterations have been performed [7].

The densities formed by the mixture models can be numerically integrated over any region of interest. In particular, it is possible to calculate the probability of observing an error magnitude larger than a desired threshold by numerically integrating over all regions of the probability density that are outside the threshold's bound:

$$P(e^p > e_{max}^p) = \int_{e^p > e_{max}^p} P_p(e^p) de^p \tag{11}$$

$$P(e^v > e_{max}^v) = \int_{e^v > e_{max}^v} P_v(e^v) de^v$$

If these position and velocity thresholds are set to be the maximum resolution e_{max}^p and e_{max}^v of a particular sensor, then the numerical integrations give the probability of that sensor detecting an error between the states of the two dynamics models. This gives a measure of the validity of approximating dynamics model 1 with dynamics model 2 by computing the probability of observing an error in the sensors used to measure the true system. This method for testing model validity is summarized in Table II.

TABLE II

STEPS TO VERIFY DYNAMICS MODEL APPROXIMATIONS

1) Pick a set of N particles $\vec{x}_i(0)$ according to the known initial distribution with covariance $P(0)$.
2) Evolve particles to the desired simulation time using Table I.
3) Calculate the set of error vectors $\vec{e}_i(k) = (\vec{e}_i^{\,p} \quad \vec{e}_i^{\,v})^T$ according to equation (5).
4) Calculate the magnitudes of the position and velocity components of the error vectors $e_i^p(k)$ and $e_i^v(k)$ at a desired time index k.
5) Fit a Gaussian mixture model to the set of position magnitudes $e^p(k)$ and another mixture model to the set of velocity magnitudes $e^v(k)$ using equations (7) - (9).
6) Calculate the probability that the error has grown larger than the sensor's position resolution: $P(e^p(k) > e_{max}^p)$, and velocity resolution $P(e^v(k) > e_{max}^v)$ using equation (11).

III. APPLICATION TO L2 LIBRATION PT ENVIRONMENT

A. Circular Restricted Three Body Problem

The error probability evolution technique is now applied to a satellite formation near the Sun - Earth / Moon L2 libration point. The L2 point is one of five points of equilibrium in the combined gravitational environment of the Sun and the Earth / Moon system [1]. Figure 1 shows that the L2 point, along with L1 and L3, form a set of libration points that are collinear with the Sun and the Earth / Moon barycenter [8]. A satellite placed near one of these collinear points has well-characterized dynamics provided it is considered with several assumptions [1]:

1) The Sun and the Earth / Moon system travel in circular orbits about their barycenter.
2) The satellite is sufficiently small as to have no effect on the motion of the Sun or Earth / Moon.
3) No other forces affect the system.

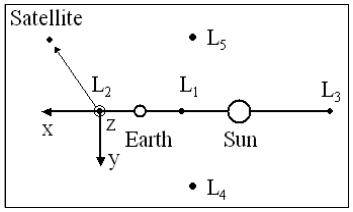

Fig. 1. Geometry of the Sun-Earth libration points with coordinate frame centered on L2 and rotating about the Sun / Earth barycenter

Under these assumptions, the problem is known as the circular restricted three-body problem (CRTBP) [1]. The full dynamics for this problem may be derived from the

Lagrangian. In Ref. [1], for example, the satellite is considered in a coordinate frame that rotates about the Sun / Earth barycenter, centered on the L2 point:

$$\ddot{\rho}_x = \dot{\rho}_y + \frac{\partial L}{\partial \rho_x}, \quad \ddot{\rho}_y = -\dot{\rho}_x + \frac{\partial L}{\partial \rho_y}, \quad \ddot{\rho}_z = \frac{\partial L}{\partial \rho_z} \tag{12}$$

L is the Lagrangian for the system, used here with the same form and notation used in [1]:

$$L = \frac{1}{2}\left(\dot{\vec{\rho}} - K\vec{\rho}\right)^2 + \alpha_2 \frac{\rho_x}{\|\vec{r}_1\|} + \tag{13}$$
$$+ \frac{\mu}{\|\vec{r}_1\|^3}\frac{1}{\|\vec{\rho} + \vec{e}_1\|} + \frac{1-\mu}{\|\vec{r}_1\|^2\|\vec{r}_2\|}\frac{\|\vec{r}_2\|/\|\vec{r}_1\|}{\|\vec{\rho} + \frac{\|\vec{r}_2\|}{\|\vec{r}_1\|}\vec{e}_1\|}$$

where $\vec{\rho}$ is a 3 element vector of normalized position with respect to the L2 point, ρ_x, ρ_y, and ρ_z are the x, y, and z components of the vector $\vec{\rho}$, respectively, and:

$$K = \begin{pmatrix} 0 & 1 & 0 \\ -1 & 0 & 0 \\ 0 & 0 & 0 \end{pmatrix}, \vec{e}_1 = \begin{pmatrix} 1 \\ 0 \\ 0 \end{pmatrix}$$

The parameter $\alpha_2 = 1.010075174$ is such that $\alpha_2\vec{e}_1$ is the location of L2 with respect to a rotating coordinate system centered at the Sun / Earth - Moon barycenter and normalized by 1 AU. The parameter $\mu = 3.0404 \cdot 10^{-6}$ is the ratio of the Earth - Moon system's mass to the total mass of the Sun / Earth - Moon system, using the stellar constants given in [2]. The parameters $\vec{r}_1$ and $\vec{r}_2$ are vectors from the L2 point to the Earth and the Sun, respectively. Both are in the dimensionless coordinate frame of [1]. Their values in this dimensionless coordinate frame are given below, again using stellar constants from [2]:

$$\vec{r}_1 = \begin{pmatrix} -0.0100782144 \\ 0 \\ 0 \end{pmatrix}, \vec{r}_2 = \begin{pmatrix} -1.0100782144 \\ 0 \\ 0 \end{pmatrix}$$

The form and notation of the above dynamics equation are taken from [1] and apply to the dimensionless coordinate frame given in that same paper. These coordinates relate to the physical coordinates of Figure 1 by the following transformation [1]:

$$\begin{aligned} \text{position (in km): } \vec{x} &= T_x \cdot \vec{\rho} \\ \text{velocity (in km/s): } \vec{v} &= T_v \cdot \dot{\vec{\rho}} \end{aligned} \tag{14}$$

where $\vec{x}$ and $\vec{v}$ are position and velocity perturbations from the L2-centered rotating coordinate frame of Figure 1, and $T_x \equiv \|\vec{r}_1\| \cdot 149597870$, $T_v \equiv \|\vec{r}_1\| \cdot 29.784735$.[1]

In contrast to the full dynamics of equation (12), an alternative representation is to expand the Lagrangian in a series of Legendre polynomials, giving a different form of the dynamics [1], [8], [9]:

$$\ddot{\vec{\rho}} = 2K\dot{\vec{\rho}} - K^2\vec{\rho} + \sum_{n=2}^{\infty} n c_n P_n\left(\frac{\rho_x}{\|\vec{\rho}\|}\right)\|\vec{\rho}\|^{n-2}\vec{\rho} +$$
$$+ \sum_{n=2}^{\infty} c_n P_n'\left(\frac{\rho_x}{\|\vec{\rho}\|}\right)\|\vec{\rho}\|^{n-2}\left(\|\vec{\rho}\|\vec{e}_1 - \frac{\rho_x}{\|\vec{\rho}\|}\vec{\rho}\right) \tag{15}$$

where the notation is the same as in equation (12), P_n is the n^{th} Legendre polynomial, and:

$$c_n = (-1)^n \frac{\mu}{\|\mathrm{r}_1\|^3} + (-1)^n \frac{(1-\mu)\|\mathrm{r}_1\|^{\mathrm{n}-2}}{\|\mathrm{r}_2\|^{\mathrm{n}+1}}$$

The transformation of equation (14) may be applied to convert these dimensionless coordinates into the physical coordinates of Figure 1. This summation form is classically used to search for closed-form orbits near the libration points, which are discussed in the next section.

B. Halo Orbits

In early studies of the libration points [8], [9], the CRTBP dynamics of equation (15) were truncated at degree 3; perturbation analysis of this truncated system yielded families of so-called *halo orbits* near the three collinear libration points. These closed-form halo orbits are characterized by an orbital parameter Ax or Az: the in-plane x position or the out-of-plane z position at the y axis crossing, and n, the orbit family [1]. Though satellite dynamics near these halo orbits are unstable, they are known to be slow relative to the Earth. This makes them attractive for longterm space telescope missions in which low fuel maneuvers, consistent environments, and relatively small disturbances are essential [2]. For this study, a halo orbit based on future formation missions near L2 [10] was constructed using the truncated dynamics of [8] and [9]. Although this approximation is a closed-form orbit derived from the dynamics of equation (15), it does not represent a solution to the full CRTBP dynamics of equation (12) due to the differences between the truncated dynamics and the full dynamics. Nonetheless, this approximate halo orbit may be used as an initial guess to compute the true halo orbit using the full dynamics of equation (12) and the general iterative scheme described in [1]; the true halo orbit lies at least 20000 km farther from the L2 point in the xy and yz planes than its reduced order counterpart. This particular halo orbit is chosen based on observations in Ref. [11] that simulation results obtained from this halo orbit in the full CRTBP dynamics tend to hold under the true dynamics near the L2 point.

Because closed-form orbital solutions are not necessary for this study, the full dynamics of equation (12) are used for numerical integration instead of the Legendre series form of the dynamics. This eliminates errors between the approximate orbits from Ref. [8], [9] and the actual orbits.

C. Disturbance Model of the L2 Environment

In addition to the CRTBP dynamics of equation (12), there are two significant sources of disturbances in the L2 environment that must be considered: solar pressure and gravitational perturbations [2]. Gravitational perturbations result primarily from variations in the location of the L2 point caused by the Moon's orbit, perturbations due to the Earth's eccentricity in its orbit about the Sun, and perturbations from other planets. To characterize these disturbances in simulation, the worst case disturbing

acceleration (in m/s^2) was obtained for each coordinate axis of the reference frame of Figure 1 [2]. The bound on each axis was then taken as the 3σ value for the disturbance along that axis. The initial distribution of the disturbance was assumed Gaussian, and it was kept constant during the simulation to account for the fact that the gravitational disturbance is, to a good approximation, constant over short timescales. The covariance for the gravitational perturbation $\vec{w}_G$ is given below:

$$Q_{cts} = diag(1.535{\cdot}10^{-13}, 9.727{\cdot}10^{-14}, 9.604{\cdot}10^{-16}) \quad (16)$$

The subscript cts is used because the perturbations are represented in continuous time in this simulation. This disturbance is assumed to act directly on the velocity states only. For the satellite simulations, the continuous satellite dynamics are numerically integrated directly, so no discrete time approximation was used. That is, the dynamics are written in the form of equation (1), and that equation is numerically integrated directly using B_{cts} and $\vec{w}_{cts}$ without explicitly creating $B(t_k)$ and $\vec{w}(t_k)$.

The second disturbance, solar pressure, was computed according to the radial force model outlined in [2]:

$$\vec{w}_{SRP} = \frac{1367 \cdot 2A}{mcR^2}\hat{r} \quad (17)$$

where A is the satellite's sunshade area, m is the satellite's mass, c is the speed of light, R is the distance from the satellite to the Sun, in AU, and $\hat{r}$ is a unit vector pointing away from the Sun along the line between it and the satellite. This solar pressure model assumes that the satellite has a perfectly reflective sunshade perpendicular to the direction of the Sun's rays.

The initial state error covariance was assumed to be consistent with the capabilities of the Autonomous Formation Flying sensor (AFF), one of the only sensor schemes currently being tested for use in satellite formation flying at the libration points [12]. The absolute tolerances given in [12] were modeled as the 3σ values of the satellite states (in m and m/s), so the initial state error covariance was assumed to be Gaussian, with:

$$P(0) = \begin{bmatrix} 4.4{\cdot}10^{-5} \cdot I_{3\times3} & 0 \\ 0 & 1.1{\cdot}10^{-7} \cdot I_{3\times3} \end{bmatrix}$$

D. Validation of Relative Satellite Model

Many future L2-based space telescope missions will require arrays of satellites flying in precisely controlled formations [13]. Nonetheless, the satellite dynamics are nonlinear, so applying robust control tools is difficult. Because the time evolution of these dynamics are 'slow,' it is purported that double integrator approximations to relative satellite dynamics could be used, as was done in [3] for an Earth trailing orbit. However, the window of validity of such approximations is not known for the L2 environment.

The approach here is to use the model error evaluation process developed in section II in order to characterize the window of validity of these approximate models at L2. Specifically, this section shows the validity of double integrator approximations to the relative satellite dynamics of two satellites flying in formation.

The truth model for the j^{th} satellite Sj includes solar radiation pressure, gravitational disturbances, and the effects of the CRTBP dynamics:

$$\frac{d}{dt}\begin{pmatrix}\vec{x}\\ \dot{\vec{x}}\end{pmatrix}_{Sj} = \frac{d}{dt}\begin{pmatrix}T_x\cdot\vec{\rho}\\ T_v\cdot\dot{\vec{\rho}}\end{pmatrix}_{Sj} + \begin{pmatrix}\vec{0}\\ \vec{w}_G\end{pmatrix} + \begin{pmatrix}\vec{0}\\ \vec{w}_{SRP}\end{pmatrix}_{Sj} \quad (18)$$

where the transformations $\vec{x} = T_x \cdot \vec{\rho}$ and $\vec{v} = T_v \cdot \dot{\vec{\rho}}$ from equation (14) are used to write the satellite state $\vec{\rho}$ and $\dot{\vec{\rho}}$ in the physical coordinates of Figure 1, and the inputs $\vec{w}_G$ and $\vec{w}_{SRP}$ are the disturbances from gravitational and solar pressure perturbations of equations (16) and (17), respectively. Solar radiation pressure parameters were taken from [3].

In contrast, the double integrator model assumes that satellite dynamics can be approximated as a double integrator in the rotating coordinate frame of Figure 1. The model also includes identical gravity and solar pressure disturbances as those driving the truth model of equation (18). The dynamics of the j^{th} satellite are represented in the double integrator 'DI' dynamics as:

$$\frac{d}{dt}\begin{pmatrix}\vec{x}_{DI}\\ \dot{\vec{x}}_{DI}\end{pmatrix} = \begin{pmatrix}\vec{0}\\ \vec{w}_G\end{pmatrix} + \begin{pmatrix}\vec{0}\\ \vec{w}_{SRP}\end{pmatrix} \quad (19)$$

Six separate satellites were simulated in this environment in order to evaluate formations of spacecraft near L2. Each satellite was displaced from the nominal formation center along the positive or negative direction of one coordinate axis. An arbitrary point on the reference halo orbit was taken as the formation center: $(x, y, z, \dot{x}, \dot{y}, \dot{z})^T \approx (-165000, 679000, 13400, 0.078, 0.072, -0.073)^T$ (km and km/s). The satellites' initial states relative to the formation center are listed in the table below, along with the other simulation parameters. The orbital parameters given below were used to generate a halo orbit using Richardson's approximation to the reference halo orbit; that approximation was then used to generate the corresponding reference halo orbit. The initial states given below are relative to the formation center.

			(20)
In-plane orbital radius Ax	$\approx$	220000 km	
Out-of-plane orbital radius Az	$\approx$	184000 km	
Orbit family n	$=$	1	
Satellite mass m	$=$	700 kg	
Sunshade area A	$=$	$\pi\,(15/2)^2\,m^2$	
Simulation time	$=$	8 hours	
Number of particles N	$=$	500 particles	
Initial state $(x, y, z, \dot{x}, \dot{y}, \dot{z})^T$	$=$	$(500m, 0, 0, 0, 0, 0)^T_{S1}$	
Initial state $(x, y, z, \dot{x}, \dot{y}, \dot{z})^T$	$=$	$(-500m, 0, 0, 0, 0, 0)^T_{S2}$	
Initial state $(x, y, z, \dot{x}, \dot{y}, \dot{z})^T$	$=$	$(0, 500m, 0, 0, 0, 0)^T_{S3}$	
Initial state $(x, y, z, \dot{x}, \dot{y}, \dot{z})^T$	$=$	$(0, -500m, 0, 0, 0, 0)^T_{S4}$	
Initial state $(x, y, z, \dot{x}, \dot{y}, \dot{z})^T$	$=$	$(0, 0, 500m, 0, 0, 0)^T_{S5}$	
Initial state $(x, y, z, \dot{x}, \dot{y}, \dot{z})^T$	$=$	$(0, 0, -500m, 0, 0, 0)^T_{S6}$	
Number of Gaussians M	$=$	25	

From the simulation geometry, each two-satellite formation has a formation radius of either 1 km or $0.5\sqrt{2}$ km, depending on whether the two satellites were displaced along the same axis or different axes; both of these formation sizes are comparable to the proposed size of future formation flying telescopes [3]. Each of these individual satellites is simulated separately according to the algorithm of Table I, and the dynamics model error analysis is performed on the relative dynamics between each pair of satellites. For formation analysis, the particles of the each pair of satellite models are subtracted to yield relative states:

$$\begin{aligned} \vec{x}_{i,rel} &= \vec{x}_{i,S1} - \vec{x}_{i,S2} \\ \vec{v}_{i,rel} &= \vec{v}_{i,S1} - \vec{v}_{i,S2} \end{aligned} \tag{21}$$

where i indicates the i^{th} particle, and 'S1' and 'S2' indicate which two satellites are being compared. For each pair of satellites, two sets of relative states are created: one in which the satellites are driven under the full dynamics of equation (18), and another in which the satellites are driven under the double integrator dynamics of equation (19). In particular, the dynamics $f_1(\vec{x})$ of equation (4) correspond to the relative states generated by driving two satellites by the full dynamics of equation (18), while the dynamics $f_2(\vec{x})$ of equation (4) correspond to the relative states generated by driving two satellites by the double integrator dynamics of equation (19).

These two sets of relative states were compared using the algorithm of Table II. The algorithm was applied to the error between the true relative state and the double integrator approximation. The error thresholds were set to be $e^p_{max} = 0.02m$ and $e^v_{max} = 0.001\frac{m}{s}$ and correspond to the smallest position and velocity measurable by the AFF sensor [12]. Any model errors below these thresholds would not be observed by the AFF sensor.

The simulations show that the formation between satellites in the $+x$ and $-x$ directions (satellites S1 and S2 in equation (20)), are most likely to have a detectable error between the double integrator model and the true dynamics at this point in the reference halo orbit. Figure 2 shows the results of the relative dynamics simulation, with the worst formation drawn with o's and x's on position and velocity error, respectively. Results show that a double integrator approximation to relative satellite dynamics between the pairs of simulated satellites may be used at least for two hours with approximately 1% probability of a position error of detectable magnitude, and the probability of error quickly increases after this two hour mark. The probability of a detectable velocity error, in contrast, remains near zero for the entire simulation.

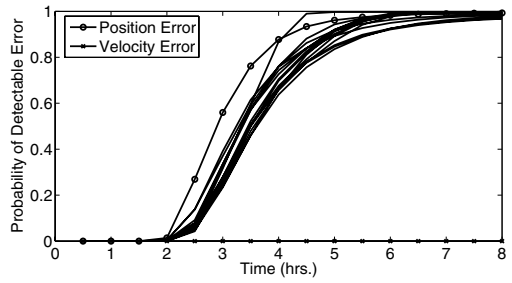

Fig. 2. Probability of detectable errors in relative satellite dynamics

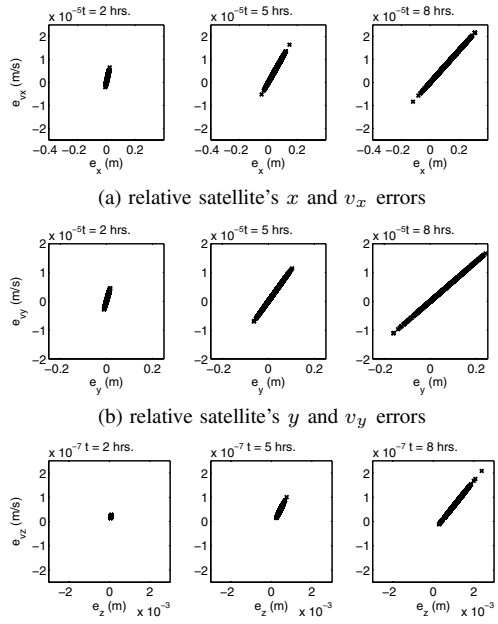

(a) relative satellite's x and v_x errors

(b) relative satellite's y and v_y errors

(c) relative satellite's z and v_z errors

Fig. 3. Evolution of worst simulated formation's position and velocity errors over 8 hours

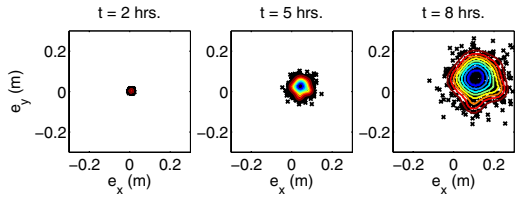

Fig. 4. Evolution of equiprobability curves for worst simulated formation's x and y position errors over 8 hours

Figures 3a-c show the distributions of the relative state errors for the worst satellite formation. The relative errors in the x and y axes expand significantly over the course of the simulation. In contrast, the errors in the z axis remain smaller and more tightly clustered, and the mean drifts significantly compared to the size of the distribution. Figure 4 plots the equiprobability curves of an $M = 20$ Gaussian mixture model whose component Gaussians have covariances of the form $\sigma_i^2 \cdot I$. The nearly-elliptical curves are plotted at 10% intervals and show that the distribution of the relative state errors remains nearly Gaussian during the simulation. Because of this fact, the number of Gaussians M is found to have negligible effect on the shape of Figure 2 for M between 1 and 250 Gaussians. The equiprobability curves also show the significant expansion of errors in the x and y axes, as well as a drift in the mean of these errors. These dynamical effects can be explained with

the difference between the true and simplified dynamics models. Because the simplified dynamics model does not include the Earth's gravity, each satellite in the formation experiences an additional gravitational force in the true dynamics model. This effect causes the means of the relative errors to drift as observed in Figures 3a-c, and represents the difference between the dynamics of the halo orbit and the double integrator environment. The fact that the satellite formation aligned with the $+x$ and $-x$ directions are most likely to have a detectable error can be explained from the dynamics equations themselves. An evaluation of the particles of each formation at the start of the simulation shows that the satellites displaced along the x axis experience a relative acceleration of nearly twice the magnitude than those displaced along the y or z axes at this point in the reference halo orbit. These results suggest that formations primarily oriented along the x axis will suffer from greater formation model error than those in other orientations at this particular point in the reference orbit.

In contrast to the worst formation, the formation in which model validity lasts the longest with small probability of detectable error is the formation with one satellite along the $-y$ direction and one satellite along the $-z$ direction. At the beginning of the simulation, this formation experiences relative forces that are on average about three times smaller than those experienced by the worst formation. However, despite the significant differences in relative forces, the detectable error probability still diverges only 30 minutes after that of the worst formation.

E. Factors Influencing Model Validity at L2

The results of section III-D show that at a particular point on a reference halo orbit, the double integrator model for satellite formation dynamics holds for approximately 2 hours with low probability of detectable error between it and the true relative dynamics. This section further examines the effects of several factors that influence the position probability curves of Figure 2. The velocity probability curves are not plotted, as they are negligible for the duration of each simulation and not affected by any experimental variations explored in this section.

The first factor examined was the effect of varying the size of the satellite formation. In section III-D, all two-satellite formations were either 1 km or $0.5\sqrt{2}$ km. In this study, the worst formation was first reduced so its two satellites were separated by 100 m. In this smaller formation, the satellites were shifted relative to the formation center along the x axis by only ± 50 m instead of ± 500 m as was done in section III-D. Next, the pair of satellites was separated by 2 km; in this formation, the satellites were shifted ± 1 km from from the formation center along the x axis at the outset. The satellites were simulated with these new formation sizes, and all other simulation parameters remained the same as in equation (20). Position error probability curves were computed as in section III-D, and are shown in Figure 5. The results show that formation size plays a significant role in determining the window of validity of the double integrator approximation for formation dynamics near L2. The double integrator model for the 2 km formation holds only for 1.5 hours and then degrades rapidly, while the same model for the 100 m formation holds for 2.5 hours and degrades much slower over the simulation. Since the simulations for the various formation sizes all share the same sensor noise and disturbance parameters, the differences in the error probability curves of Figure 5 are due to the difference between the L2 dynamics of equation (12) and the double integrator model of equation (19).

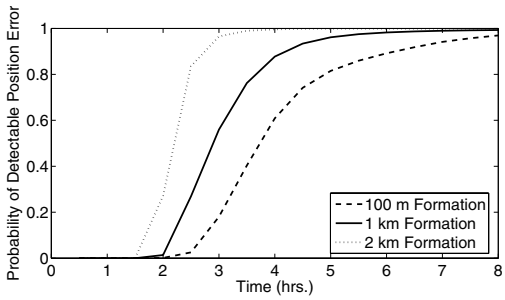

Fig. 5. Effects of varying formation size for worst satellite formation

These results show the L2 dynamics begin to influence simplified model validity after about 2 hours using the above simulation parameters and different formation sizes. However, Figure 5 gives the worst case scenario, because it includes sensor noise, solar pressure disturbances, and gravitational perturbations. To examine the effect of the L2 dynamics alone, the two-satellite formation was simulated deterministically at different formation sizes. That is, each satellite was simulated with no sensor noise, no solar pressure, and no gravitational disturbances. The same errors were then calculated between the full dynamics model and the double integrator model. Figure 6 shows how those errors evolve in time. In the absence of sensor noise and other disturbances, position error hits the $e^p_{max} = 2$ cm mark at about 2 hours, 10 minutes for a 2 km formation, about 3 hours 5 minutes for the 1 km formation, and it does not cross the 2 cm mark for the 100 m formation over the 8 hour simulation. None of the formation sizes crossed the $e^v_{max} = 1mm/s$ error limit during the simulation; velocity errors were at least one order of magnitude lower than the limit during the entire simulation. Additionally, the same deterministic curves computed with gravitational perturbations and solar pressure differ from the original by 10^{-7} m at the end of the simulation; the effects of solar pressure and gravitational perturbations are therefore negligible for these formation sizes and time horizons. Comparing these results with Figure 5 yields an important conclusion: sensor noise causes the double integrator model's validity to fail 30 minutes earlier than could possibly be expected for the 2 km formation, 1 hour earlier for the 1 km formation, and at least 5 hours earlier for the 100 m formation. In other words, at the formation sizes being considered for future L2

space telescopes, sensor noise dominates formation model validity over solar pressure, gravitational perturbations, and even the L2 dynamics.

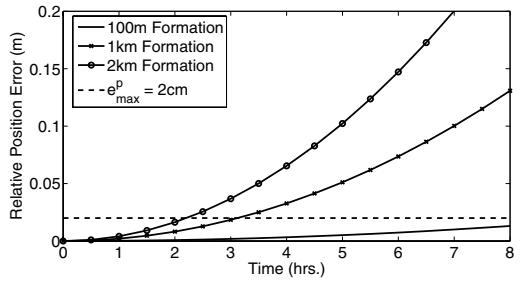

Fig. 6. Evolution of worst simulated formation's deterministic position errors over 8 hours

To see whether position or velocity sensor error is the dominating factor over these short time horizons, the same 1 km formation was simulated with varying levels of sensor noise. To accomplish this, each of the position and velocity sensor noise standard deviations was increased or decreased separately by a factor of 10. The position probability curves for the different levels of velocity noise are shown in Figure 7. The effects of changing sensor position error are not plotted; changing sensing accuracy by even a factor of 10 changes the curves by $\Delta p \approx 0.01$. In contrast, changing velocity sensing accuracy by a factor of 10 causes model validity to drop after 30 minutes or nearly 3 hours, depending on whether error is increased or decreased. This shows that velocity error is the dominating factor in determining model validity with current formation sensing capabilities. Notice that when velocity error is decreased, the double integrator remains valid for this formation for nearly 3 hours, the amount of time suggested by Figure 6a for a 1 km formation. In other words, current velocity sensing errors can be reduced significantly before CRTBP dynamics become the dominant factor driving model validity.

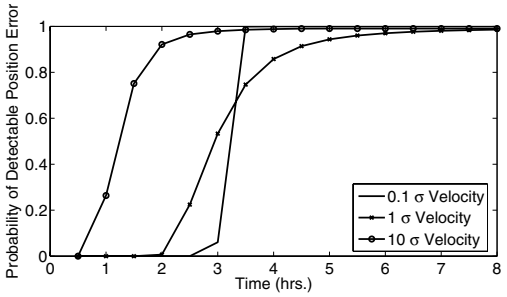

Fig. 7. Effects of varying velocity sensor noise for a 1 km formation

IV. Conclusions

An approach has been developed to analyze the error between two models (typically a simple model and a complex model), in terms of an error probability density function and probability over time. The technique uses particles to evolve nonlinear probability density functions through nonlinear models. The approach is especially useful in applications where the control design model is an approximate version of the truth model. In these cases, confidence in the approximation can be probabilistically evaluated. The approach was shown to give insightful results for L2 formation dynamics.

The approach has shown for typical halo-orbit based satellite formations that at the particular point selected, the double integrator approximation to relative satellite dynamics near the L2 point may be used for at least 2 hours with low probability of a detectable error from existing formation sensors. The simulations have also shown that at the formation sizes under consideration for future space telescopes, sensor-based noise in satellite velocity dominates all other sources of model error near L2. Improved velocity sensing will keep approximations valid over longer time horizons, especially for formations at or under 1 km in size. Additionally, it was also shown that L2 based orbits and formations have preferred orientations in which the double integrator approximation holds for longer periods of time. This suggests that formation control strategies might benefit from accounting for or taking advantage of these preferred orientations.

V. Acknowledgments

This material is based upon work supported under a National Science Foundation Graduate Research Fellowship and the NASA CETDP Program.

References

[1] R. Thurman and P. Worfolk, "The geometry of halo orbits in the circular restricted three-body problem," University of Minnesota: Geometry Center Research Report GCG95, 1996.

[2] S. Evans, "Natural environment near the sun/earth-moon L2 libration point," Marshall Space Flight Center, 2003.

[3] D. Scharf, F. Hadaegh, and B. Kang, "On the validity of the double integrator approximation in deep space formation flying," Formation Flying Symposium, Toulouse, France, 2002.

[4] D. Kirk, *Optimal Control Theory: An Introduction*. Prentice-Hall, 1970.

[5] R. Van der Merwe and E. Wan, "Sigma-point kalman filters for probabilistic inference in dynamic state-space models," Workshop on Advances in Machine Learning, Montreal, 2003.

[6] M. Arulampalam, S. Maskell, N. Gordon, and T. Clapp, "A tutorial on particle filters for online nonlinear / non-guassian bayesian tracking," *IEEE Transactions on Signal Processing*, vol. 50, no. 2, 2002.

[7] C. Bishop, *Neural Networks for Pattern Recognition*. Oxford University Press, 1995.

[8] D. Richardson, "Analytic construction of periodic orbits about the collinear points," *Celestial Mechanics*, vol. 22, 1980.

[9] ——, "A note on a lagrangian formulation for motion about the collinear points," *Celestial Mechanics*, vol. 22, 1980.

[10] C. Beichman, G. Gómez, M. Lo, J. Masdemont, and L. Romans, "Searching for life with the Terrestrial Planet Finder: Lagrange point options for a formation flying interferometer," *Advances in Space Research*, vol. 34, 2004.

[11] G. Gómez, M. Lo, J. Masdemont, and K. Museth, "Simulation of formation flight near L2 for the TPF mission," AAS/AIAA Astrodynamics Specialist Conference, Quebec City, Canada, Paper AAS 01-305, 2001.

[12] M. Aung, G. Purcell, J. Tien, L. Young, L. Amaro, J. Srinivasan, M. Ciminera, and Y. Chong, "Autonomous formation-flying sensor for the StarLight mission," *IPN PR 42-152*, vol. October - December 2002, February 2003.

[13] C. Beichman, N. Woolf, and C. Lindensmith, "Terrestrial Planet Finder," *JPL Publication 99-003*, 1999.